PHYSICAL REVIEW D **84,** 093006 (2011)

Status of 3 + 1 neutrino mixing

Carlo Giunti*
INFN, Sezione di Torino, Via P. Giuria 1, I–10125 Torino, Italy

Marco Laveder†
Dipartimento di Fisica "G. Galilei," Università di Padova, and INFN, Sezione di Padova, Via F. Marzolo 8, I–35131 Padova, Italy
(Received 26 September 2011; published 22 November 2011)

We present an update of our analysis of short-baseline neutrino oscillation data in the framework of 3 + 1 neutrino mixing taking into account the recent update of MiniBooNE antineutrino data and the recent results of the MINOS search for ν_μ disappearance into sterile neutrinos (the more complicated 3 + 2 neutrino mixing is not needed since the *CP*-violating difference between MiniBooNE neutrino and antineutrino data has diminished). The results of our fits of short-baseline neutrino oscillation data including the MiniBooNE low-energy anomaly (now present both in the neutrino and antineutrino data) lead to a strong tension between appearance and disappearance data. Hence, it seems likely that the low-energy anomaly is not due to $\overset{(-)}{\nu}_\mu \to \overset{(-)}{\nu}_e$ transitions. Excluding the MiniBooNE low-energy anomaly, appearance and disappearance data are marginally compatible. The global analysis has the best-fit point at $\Delta m^2_{41} \approx 5.6\ \mathrm{eV}^2$, which is rather large in comparison with cosmological bounds, but there are three regions within 1σ at $\Delta m^2_{41} \approx 1.6,\ 1.2,\ 0.91\ \mathrm{eV}^2$. We also show that the data on the Gallium neutrino anomaly favor values of Δm^2_{41} larger than about $1\ \mathrm{eV}^2$.

DOI: 10.1103/PhysRevD.84.093006 PACS numbers: 14.60.Pq, 14.60.Lm, 14.60.St

I. INTRODUCTION

The possible existence of sterile neutrinos is an exciting possibility which could open a powerful window on our view of the physics beyond the standard model. The short-baseline (SBL) neutrino oscillation experiment LSND [1] discovered in the late 90's a signal which can be due to $\bar\nu_\mu \to \bar\nu_e$ oscillations generated by a neutrino squared-mass splitting $\Delta m^2_{\mathrm{SBL}}$ of the order of $1\ \mathrm{eV}^2$, which is much larger than the well-established solar (SOL) and atmospheric (ATM) squared-mass splittings, $\Delta m^2_{\mathrm{SOL}} = (7.6 \pm 0.2) \times 10^{-5}\ \mathrm{eV}^2$ [2] and $\Delta m^2_{\mathrm{ATM}} = 2.32^{+0.12}_{-0.08} \times 10^{-3}\ \mathrm{eV}^2$ [3]. In order to have more than two independent squared-mass splittings, the number of massive neutrinos must be larger than 3. In this case, the flavor neutrino basis is composed by the three known active neutrinos ν_e, ν_μ, ν_τ and by one or more sterile neutrinos ν_{s1}, ν_{s2}, ..., which do not have standard weak interactions and do not contribute to the number of active neutrinos determined by CERN LEP experiments through the measurement of the invisible width of the Z boson, $N_a = 2.9840 \pm 0.0082$ [4].

Schemes of neutrino mixing with sterile neutrinos have been studied by several authors (see Refs. [5–8]), with more attention to the simple schemes with one or two sterile neutrinos (four- and five-neutrino mixing, respectively). Since the three active neutrinos must have large mixing with the three massive neutrinos which generate $\Delta m^2_{\mathrm{SOL}}$ and $\Delta m^2_{\mathrm{ATM}}$ and no effect of sterile neutrinos has been seen in solar and atmospheric neutrino data, the mixing schemes with sterile neutrinos must be perturbations of the standard three-neutrino mixing scheme in which the three active neutrinos ν_e, ν_μ, ν_τ are superpositions of three massive neutrinos ν_1, ν_2, ν_3 with respective masses m_1, m_2, m_3, such that $\Delta m^2_{\mathrm{SOL}} = \Delta m^2_{21}$ and $\Delta m^2_{\mathrm{ATM}} = |\Delta m^2_{31}| \simeq |\Delta m^2_{32}|$, with $\Delta m^2_{kj} = m^2_k - m^2_j$. Moreover, standard analyses of the cosmic microwave background and large-sScale structures data constrain the neutrino masses in the case of three-neutrino mixing to be much smaller than 1 eV [9–12] and are compatible with the existence of one or two sterile neutrinos which have been thermalized in the early Universe [13] only if the masses of the additional, mainly sterile, massive neutrinos are smaller than about 1 eV [14–19]. Also, big-bang nucleosynthesis data are compatible with the existence of sterile neutrinos which have been thermalized in the early Universe [20,21], with the indication however that schemes with more than one sterile neutrino are disfavored [19,22]. Hence, the schemes with sterile neutrinos which are currently under consideration are the 3 + 1 and 3 + 2 schemes in which ν_e, ν_μ, ν_τ are mainly mixed with ν_1, ν_2, ν_3, whose masses are much smaller than 1 eV, and there are one or two additional massive neutrinos, ν_4 and ν_5, which are mainly sterile and have masses of the order of 1 eV. Short-baseline oscillations corresponding to the LSND $\bar\nu_\mu \to \bar\nu_e$ signal are generated by the large squared-mass differences Δm^2_{41} and Δm^2_{51}.

The LSND signal was not seen in the KARMEN $\bar\nu_\mu \to \bar\nu_e$ [23], NOMAD $\nu_\mu \to \nu_e$ [24], and MiniBooNE

*Also at Department of Theoretical Physics, University of Torino, Italy.
giunti@to.infn.it
†laveder@pd.infn.it

$\nu_\mu \to \nu_e$ [25] short-baseline experiments. However, in July 2010 the interest in the LSND signal has been revived by the observation of a compatible signal in the MiniBooNE $\bar{\nu}_\mu \to \bar{\nu}_e$ short-baseline experiment [26]. The MiniBooNE and LSND antineutrino data have been analyzed in several papers in conjunction with the data of other short-baseline experiments in the framework of 3 + 1 and 3 + 2 schemes [27–30]. In this paper, we update the 3 + 1 analysis presented in Ref. [30] by taking into account the update of MiniBooNE antineutrino data presented in Refs. [31,32] and the recent results of the MINOS search for ν_μ disappearance into sterile neutrinos [33].

In 3 + 1 schemes, we have the squared-mass hierarchy

$$\Delta m^2_{21} \ll \Delta m^2_{31} \ll \Delta m^2_{41}, \tag{1}$$

and we consider four-neutrino mixing as a perturbation of three-neutrino mixing:

$$|U_{e4}|^2, \quad |U_{\mu 4}|^2, \quad |U_{\tau 4}|^2, \quad \ll 1, \quad |U_{s4}|^2 \simeq 1. \tag{2}$$

The effective flavor transition and survival probabilities in SBL experiments are given by

$$P^{\text{SBL}}_{\overset{(-)}{\nu}_\alpha \to \overset{(-)}{\nu}_\beta} = \sin^2 2\vartheta_{\alpha\beta} \sin^2\left(\frac{\Delta m^2_{41} L}{4E}\right) \qquad (\alpha \neq \beta), \tag{3}$$

$$P^{\text{SBL}}_{\overset{(-)}{\nu}_\alpha \to \overset{(-)}{\nu}_\alpha} = 1 - \sin^2 2\vartheta_{\alpha\alpha} \sin^2\left(\frac{\Delta m^2_{41} L}{4E}\right), \tag{4}$$

for $\alpha, \beta = e, \mu, \tau, s$, with

$$\sin^2 2\vartheta_{\alpha\beta} = 4|U_{\alpha 4}|^2 |U_{\beta 4}|^2, \tag{5}$$

$$\sin^2 2\vartheta_{\alpha\alpha} = 4|U_{\alpha 4}|^2 (1 - |U_{\alpha 4}|^2). \tag{6}$$

In this paper, we do not consider 3 + 2 neutrino mixing because the new MiniBooNE antineutrino data [31,32] do not show a sufficient difference from the MiniBooNE neutrino data [25] to motivate the consideration of the much more complicated 3 + 2 neutrino mixing, which could explain a difference through *CP* violation in short-baseline oscillations [27,29,30,34–37]. In Ref. [30], we have shown that such an effect would be the main motivation for preferring 3 + 2 mixing over 3 + 1 mixing.

The plan of the paper is as follows. In Secs. II and III, we describe, respectively, our analysis of the new MiniBooNE antineutrino data and that of MINOS data on the search for ν_μ disappearance into sterile neutrinos. In Sec. IV, we present the results of the global fit of short-baseline oscillation data and in Sec. V we draw our conclusions.

II. MINIBOONE

The MiniBooNE collaboration presented recently a preliminary update of their antineutrino data obtained with 8.58×10^{20} protons on target (POT) [31,32], which increases the amount of data by a factor of about 3/2 with respect to the data published in Ref. [26], which were obtained with 5.66×10^{20} POT. The new data show two interesting new features:

(1) The antineutrino data have an anomalous low-energy excess similar to that of the neutrino data [25].
(2) The $\bar{\nu}_\mu \to \bar{\nu}_e$ signal in the three energy bins from 475 MeV to 800 MeV has slightly diminished with respect to that published in Ref. [26].

The first new feature raises the interesting question if the MiniBooNE low-energy anomaly can be fitted by oscillations. In order to answer this question, we consider the fit of MiniBooNE data with and without the three low-energy bins from 200 MeV to 475 MeV. The second new feature may be the consequence of the fluctuations of the signal around the true value. A consequence of the new data is that the difference between MiniBooNE neutrino and antineutrino data has diminished, lessening the need of *CP* violation that was suggested by the previous data. Hence, there are less motivations for considering 3 + 2 neutrino mixing [27,29,30,34–37], in which $\nu_\mu \to \nu_e$ and $\bar{\nu}_\mu \to \bar{\nu}_e$ oscillations can be different if $\text{Im}[U^*_{e4} U_{\mu 4} U_{e5} U^*_{\mu 5}] \neq 0$. Moreover, as we argued in Ref. [30], 3 + 1 neutrino mixing is preferable on 3 + 2 mixing for its simplicity and for the natural correspondence of one new entity (a sterile neutrino) with a new effect (short-baseline oscillations). In Ref. [30], we have also shown that the improvement of the parameter goodness of fit in 3 + 2 schemes with respect to 3 + 1 schemes is mainly a statistical effect due to an increase of the number of parameters, in agreement with the results of Ref. [29]. Therefore, in this paper we consider only 3 + 1 neutrino mixing.

We analyzed the MiniBooNE antineutrino data extracted from the figures presented in Refs. [31,32]. We followed the method described in the MiniBooNE web page of the data release relative to Ref. [26], modified by rescaling the predicted signal by the ratio of POT. Furthermore, in order to reproduce the allowed regions in the $\sin^2 2\vartheta - \Delta m^2$ plane presented in Refs. [31,32], we increased the background uncertainty by a factor of 1.1. In the fit, we considered also the $\bar{\nu}_\mu$ data obtained with 5.66×10^{20} POT [26], which are important because of the correlated uncertainties of $\bar{\nu}_e$ and $\bar{\nu}_\mu$ data.

The results of our fits are shown in Figs. 1 and 2, respectively, for all MiniBooNE antineutrino energy bins and for the energy bins above 475 MeV. One can see that the allowed regions are similar to the corresponding ones presented in Refs. [31,32].

As one can see from Fig. 3, the low-energy anomaly is not well fitted for the best-fit value of the oscillation parameters, $\sin^2 2\vartheta_{e\mu} = 0.005$ and $\Delta m^2_{41} = 4.68\ \text{eV}^2$, but can be fitted in the case of a lower value of Δm^2_{41}. In the example A ($\sin^2 2\vartheta_{e\mu} = 0.005$ and $\Delta m^2_{41} = 0.8\ \text{eV}^2$, which is within the 68% C.L. allowed region in Fig. 1), the value of $\sin^2 2\vartheta_{e\mu}$ is the same as in the best-fit point but the

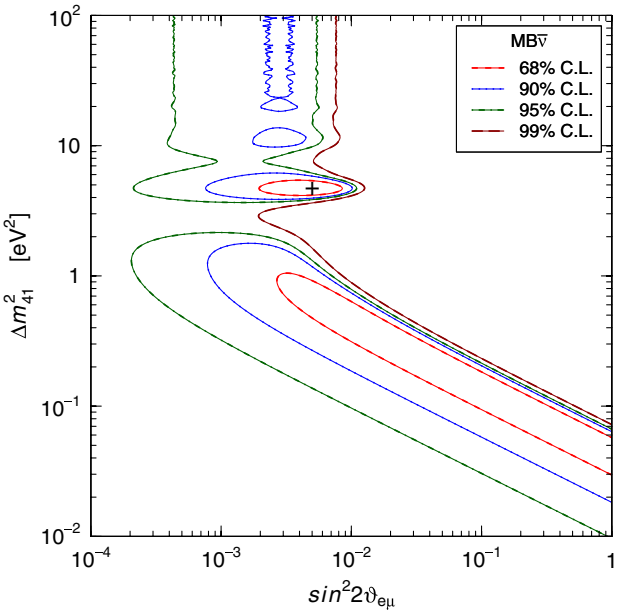

FIG. 1 (color online). Allowed regions in the $\sin^2 2\vartheta_{e\mu} - \Delta m^2_{41}$ plane obtained from the fit of MiniBooNE antineutrino data [31,32], including the low-energy bins from 200 MeV to 475 MeV. The best-fit point at $\sin^2 2\vartheta_{e\mu} = 0.005$ and $\Delta m^2_{41} = 4.68$ eV^2 is indicated by a cross.

lower value of Δm^2_{41} increases $\langle P_{\bar{\nu}_\mu \to \bar{\nu}_e} \rangle$ in the low-energy bins. In the example B ($\sin^2 2\vartheta_{e\mu} = 0.01$ and $\Delta m^2_{41} = 0.5$ eV^2, which is also within the 68% C.L. allowed region in Fig. 1), the larger value of $\sin^2 2\vartheta_{e\mu}$ and the smaller

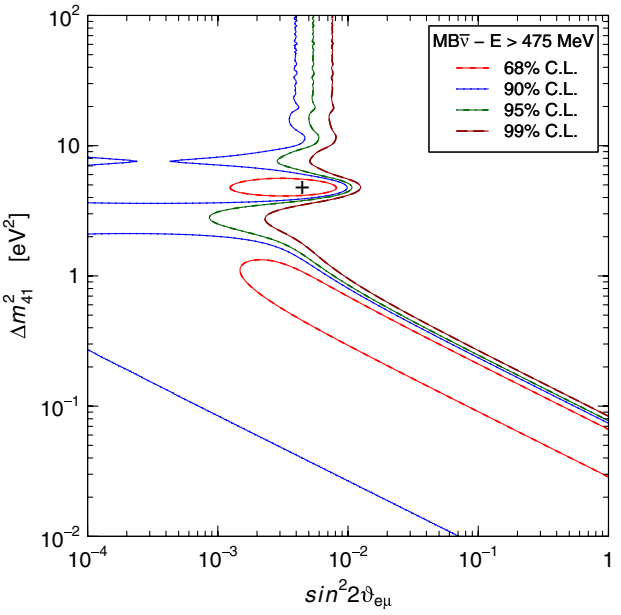

FIG. 2 (color online). Allowed regions in the $\sin^2 2\vartheta_{e\mu} - \Delta m^2_{41}$ plane obtained from the fit of MiniBooNE antineutrino data with energy $E > 475$ MeV [31,32]. The best-fit point at $\sin^2 2\vartheta_{e\mu} = 0.0045$ and $\Delta m^2_{41} = 4.79$ eV^2 is indicated by a cross.

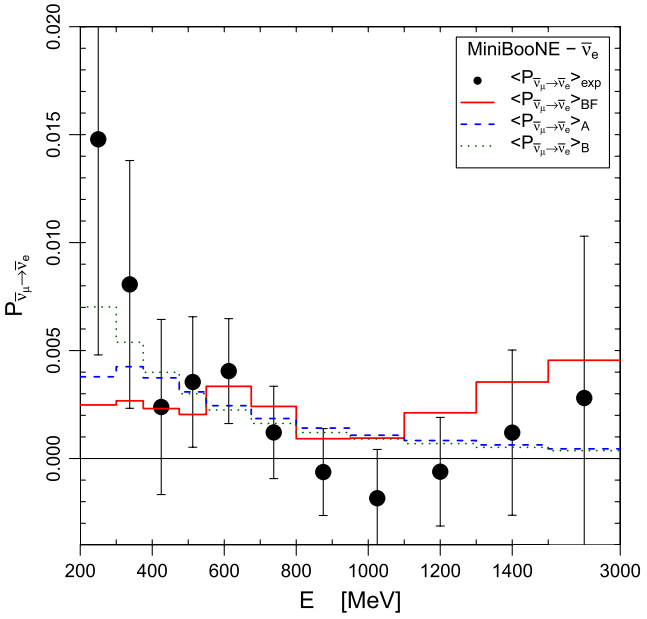

FIG. 3 (color online). Fit of MiniBooNE antineutrino data [31,32] (points with error bars). The red solid line corresponds to the best fit (BF) ($\sin^2 2\vartheta_{e\mu} = 0.005$ and $\Delta m^2_{41} = 4.68$ eV^2). The blue dashed and green dotted lines correspond, respectively, to: A: $\sin^2 2\vartheta_{e\mu} = 0.005$ and $\Delta m^2_{41} = 0.8$ eV^2; B: $\sin^2 2\vartheta_{e\mu} = 0.01$ and $\Delta m^2_{41} = 0.5$ eV^2.

value of Δm^2_{41} allow us to fit the low-energy anomaly even better. Although by eye the lines corresponding to the cases A and B may appear to fit all the MiniBooNE antineutrino data better than the best-fit line, the best-fit point has a lower value of χ^2 because of the correlations of the uncertainties of the bins, which are given by the covariance matrix of the MiniBooNE data release relative to Ref. [26].

III. MINOS

The MINOS collaboration presented recently [33] the updated results of a search for ν_μ disappearance into sterile neutrinos obtained by comparing the samples of neutral-current (NC) events measured at the near detector (ND) and far detector (FD). In the MINOS experiment, the neutrino beam is produced through the decay of pions generated by 120 GeV protons hitting a graphite target. The pions fly in a 675 m long decay pipe. The near and far detectors are located, respectively, at the distances $L_{\rm ND} = 1.04$ km and $L_{\rm FD} = 735$ km from the target. The analysis presented in Ref. [33] limits $|U_{\mu 4}|^2$ below 0.019 at 90% C.L. assuming that there are no oscillations before the near detector and that the oscillations are completely averaged in the far detector. Since the neutrino energy range goes from about 1 GeV to about 20 GeV, the first condition is satisfied for $\Delta m^2_{41} \lesssim 1$ eV^2 and the second condition is satisfied for $\Delta m^2_{41} \gtrsim 0.2$ eV^2. Hence, the

range of Δm^2_{41} for which the bound on $|U_{\mu 4}|^2$ presented in Ref. [33] is limited.

Since we consider higher values of Δm^2_{41}, we analyzed the data presented in Ref. [33] taking into account possible oscillations before the near detector. From our extraction of the data in Ref. [33], we obtained the values shown in Fig. 4 for the ratio

$$R = \frac{\langle 1 - P_{\nu_\mu \to \nu_s} \rangle_{\rm FD}}{\langle 1 - P_{\nu_\mu \to \nu_s} \rangle_{\rm ND}}. \quad (7)$$

In the fit, we considered a fully correlated 2.9% systematic uncertainty [33]. We also took into account as fully correlated the uncertainties given in Ref. [33] on the possible effect of ν_e appearance in the far detector due to $|U_{e3}|^2 < 0.040$, which is the 2010 MINOS 90% limit [38]. This value is compatible with the recent results of the T2K [39] and MINOS [40] experiments, which are in favor of ν_e appearance [41,42].

We calculated the oscillation probability at the near detector with the approximate method derived in Ref. [43], which takes into account the partial decoherence of the neutrino state at the production due to the fact that the decay length of the parent pion and the length of the decay pipe are comparable with the distance from the target to the near detector. For completeness, we took into account also possible oscillations in the far detector due to Δm^2_{41}, but we neglected for simplicity possible $\nu_\mu \to \nu_s$ transitions due to Δm^2_{31} (see Eq. (11) of Ref. [44]). This is equivalent to assuming a negligible value for $|U_{s3}|$.

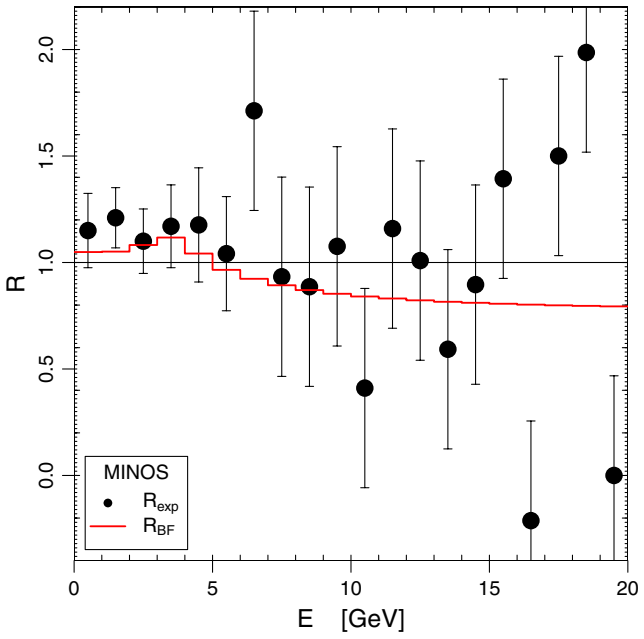

FIG. 4 (color online). Fit of MINOS data extracted from Ref. [33]. The red solid line corresponds to the best fit ($\sin^2 2\vartheta_{e\mu} = 0.005$ and $\Delta m^2_{41} = 4.68$ eV^2).

We averaged the oscillation probabilities over the neutrino flux and the neutral-current cross section, taking into account the energy resolution of the detector:

$$\langle P \rangle = I^{-1} \int dE_{\rm reco} dE_{\rm h} dE_\nu dx \frac{d^2\sigma_{\rm NC}}{dx dE_{\rm h}} \times \psi_{\rm res}(E_{\rm h}, E_{\rm reco}) \Phi_\nu(E_\nu) P(E_\nu), \quad (8)$$

where I is the same integral without $P(E_\nu)$. We took the neutrino flux $\Phi_\nu(E_\nu)$ as a function of the neutrino energy E_ν from Fig. 2.10 of Ref. [45]. The differential cross section has been approximated by the deep-inelastic cross section on an isoscalar target using the NNLO MSTW 2008 set of parton distribution functions [46]. For the energy resolution function $\psi_{\rm res}(E_{\rm h}, E_{\rm reco})$, which connects the hadronic energy $E_{\rm h}$ to the reconstructed energy $E_{\rm reco}$, we used a Gaussian distribution with standard deviation $56\%/\sqrt{E_{\rm reco}}$ [33].

Figure 5 shows the upper bound on $\sin^2 2\vartheta_{\mu\mu}$ as a function of Δm^2_{41} plane obtained with a raster scan, which can be compared with that obtained by the MINOS collaboration in Ref. [33]. One can see that for $\Delta m^2_{41} \lesssim 1$ eV^2 we have the limit $\sin^2 2\vartheta_{\mu\mu} \lesssim 0.09$ at 90% C.L., with wiggles due to oscillations in the far detector. Using Eq. (6), this limit corresponds to $|U_{\mu 4}|^2 \lesssim 0.023$, which is about the same as that obtained by the MINOS collaboration in Ref. [33]. For $\Delta m^2_{41} \gtrsim 1$ eV^2, the upper bound on $\sin^2 2\vartheta_{\mu\mu}$ rapidly disappears, in agreement with the discussion above and that in Ref. [43].

Figure 6 shows the exclusion curves in the $\sin^2 2\vartheta_{\mu\mu} - \Delta m^2_{41}$ plane obtained with a two-parameters least-squares analysis. Also, in this figure one can see that the oscillations

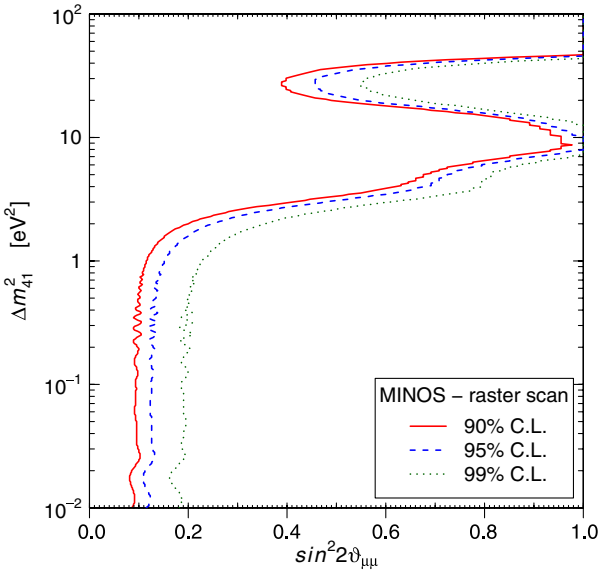

FIG. 5 (color online). Raster-scan upper bound on $\sin^2 2\vartheta_{\mu\mu}$ as a function of Δm^2_{41} plane obtained from the fit of MINOS neutral-current data [33].

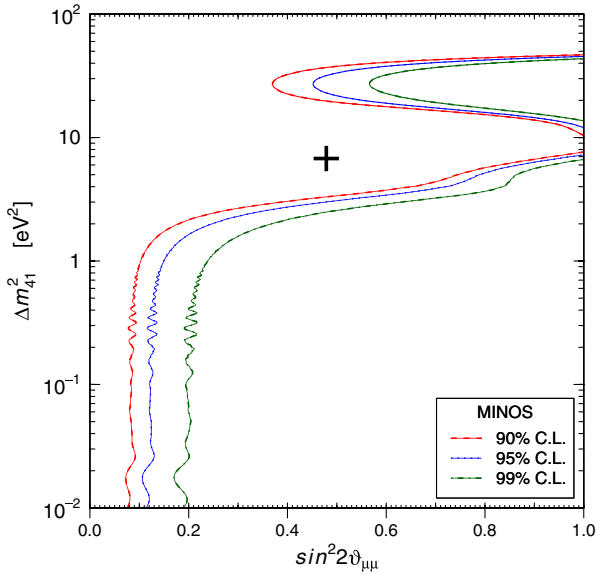

FIG. 6 (color online). Exclusion curves in the $\sin^2 2\vartheta_{\mu\mu} - \Delta m^2_{41}$ plane obtained from the fit of MINOS neutral-current data [33]. The best-fit point at $\sin^2 2\vartheta_{\mu\mu} = 0.48$ and $\Delta m^2_{41} = 6.76$ eV^2 is indicated by a cross.

in the near detector weaken the bound on $|U_{\mu 4}|^2$ for $\Delta m^2_{41} \gtrsim 1$ eV^2. The best-fit point at $\sin^2 2\vartheta_{\mu\mu} = 0.48$ and $\Delta m^2_{41} = 6.76$ eV^2 allows to fit the small positive values of R measured in the low-energy bins, which have the smaller uncertainties. This effect is in agreement with the discussion in Ref. [43], where it is explained that for a value of Δm^2_{41} such that the low-energy bins correspond to the first oscillation minimum at the near detector the denominator in Eq. (7) is smaller than the numerator, leading to $R > 1$.

IV. GLOBAL 3 + 1 FITS

In this section, we present the results of the update of our analysis in Ref. [30], which takes into account the new MiniBooNE antineutrino data discussed in Sec. II and the bound on $|U_{\mu 4}|^2$ obtained from MINOS neutral-current data in Sec. III. As in Ref. [30], we consider also the short-baseline $\overset{(-)}{\nu}_\mu \to \overset{(-)}{\nu}_e$ data of the LSND [1], KARMEN [23], NOMAD [24], and MiniBooNE neutrino [25] experiments, the short-baseline $\bar{\nu}_e$ disappearance data of the Bugey-3 [47], Bugey-4 [48], ROVNO91 [49], Gosgen [50], ILL [51], and Krasnoyarsk [52] reactor antineutrino experiments, taking into account the new calculation of the reactor $\bar{\nu}_e$ flux [53,54], which indicates a small $\bar{\nu}_e$ disappearance (the reactor antineutrino anomaly [55]), the KamLAND [56] bound on $|U_{e4}|^2$ (see Ref. [28]), the short-baseline ν_μ disappearance data of the CDHSW experiment [57], and the constraints on $|U_{\mu 4}|^2$ obtained in Ref. [37] from the analysis of the data of atmospheric neutrino oscillation experiments. We present global analyses of all these data without and with the data of Gallium radioactive source experiments (GALLEX [58–60] and SAGE [61–64]) which indicate a ν_e disappearance (the Gallium neutrino anomaly [55,65–73]). We analyze the Gallium data according to Ref. [65].

For the new MiniBooNE antineutrino data discussed in Sec. II, we consider two cases:

LOW: All MiniBooNE neutrino and antineutrino data, including the low-energy bins from 200 MeV to 475 MeV.

High (HIG): Only MiniBooNE neutrino and antineutrino data with energy $E > 475$ MeV.

Table I shows the results of our global analyses for these two cases without and with Gallium data (GAL). The corresponding allowed regions in the $\sin^2 2\vartheta_{e\mu} - \Delta m^2_{41}$, $\sin^2 2\vartheta_{ee} - \Delta m^2_{41}$, and $\sin^2 2\vartheta_{\mu\mu} - \Delta m^2_{41}$ planes are shown in Fig. 7.

From Table I, one can see that in all cases the fit of the data without oscillations is rather bad and the oscillations in the framework of 3 + 1 mixing have a good goodness of fit. The goodness of fit is larger in the HIG case than in the LOW case because the best fit of MiniBooNE data does not fit well the low-energy bins, as we have seen for the antineutrino data in Sec. II. Gallium data slightly worsen the goodness of fit because the best fit of the analysis of Gallium data [65] requires a value of $|U_{e4}|^2$, which is larger than the bound given by reactor antineutrino data (see Ref. [30]).

The best-fit value of the 3 + 1 oscillation parameters is rather stable under variations of the considered data sets. It points to a rather large value of Δm^2_{41}, which in a hierarchical scheme corresponds to $m_4 \approx 2.4$ eV. This value is in tension with the limits given by standard Λ cold dark matter (CDM) analyses of cosmological data [14–19]. If it will be confirmed by future data, it may indicate the existence of nonstandard effects in the evolution of the Universe [19]. However, as one can see from Fig. 7 there are allowed regions at $\Delta m^2_{41} \approx 1$ eV^2 which are more compatible with standard ΛCDM cosmology. For example, in the HIG fit there are three regions within 1σ at: (A) $\Delta m^2_{41} \approx 1.6$ eV^2, $\sin^2 2\vartheta_{e\mu} \approx 0.0012$, $\sin^2 2\vartheta_{ee} \approx 0.12$, $\sin^2 2\vartheta_{\mu\mu} \approx 0.037$; (B) $\Delta m^2_{41} \approx 1.2$ eV^2, $\sin^2 2\vartheta_{e\mu} \approx 0.0014$, $\sin^2 2\vartheta_{ee} \approx 0.11$, $\sin^2 2\vartheta_{\mu\mu} \approx 0.051$; (C) $\Delta m^2_{41} \approx 0.91$ eV^2, $\sin^2 2\vartheta_{e\mu} \approx 0.0020$, $\sin^2 2\vartheta_{ee} \approx 0.10$, $\sin^2 2\vartheta_{\mu\mu} \approx 0.078$.

Figure 7 shows also the 3σ contours of the regions allowed by appearance (APP) and disappearance (DIS) data. One can see that they are compatible with the global allowed regions. It is interesting to note that the values of $\sin^2 2\vartheta_{ee}$ and $\sin^2 2\vartheta_{\mu\mu}$ allowed by the analysis of appearance data can be much smaller than those allowed by the global analysis. The reason is that small values of $\sin^2 2\vartheta_{ee}$ and $\sin^2 2\vartheta_{\mu\mu}$ can be obtained not only with small values of $|U_{e4}|^2$ and $|U_{\mu 4}|^2$, respectively, but also with $|U_{e4}|^2$ and $|U_{\mu 4}|^2$ close to unity [see Eq. (6)]. Since one can fit the appearance data with $|U_{e4}|^2 \simeq 1$ and $\sin^2 2\vartheta_{e\mu} \simeq 4|U_{\mu 4}|^2$

TABLE I. Values of χ^2, number of degrees of freedom (NDF), goodness of fit (GOF) and best-fit values of the 3 + 1 oscillation parameters obtained from global fits of the data of short-baseline neutrino oscillation experiments. The first three lines correspond to the case of no oscillations (No osc.). The following nine lines correspond to the case of 3 + 1 mixing. The last three lines give the parameter goodness of fit [74] obtained by comparing the global best fit with the best fits of the appearance and disappearance data. LOW and HIG refer, respectively, to MiniBooNE data with and without the three low-energy bins from 200 MeV to 475 MeV. GAL refers to Gallium radioactive source experiment data analyzed according to Ref. [65].

		LOW	LOW + GAL	HIG	HIG + GAL
No osc.	χ^2	174.8	186.8	157.8	169.8
	NDF	133	137	127	131
	GOF	0.0088	0.003	0.033	0.013
3 + 1	$\chi^2_{\rm min}$	134.9	142.2	120.7	128.0
	NDF	130	134	124	128
	GOF	0.37	0.30	0.57	0.48
	Δm^2_{41} [eV^2]	5.6	5.6	5.6	5.6
	$\lvert U_{e4}\rvert^2$	0.032	0.037	0.033	0.038
	$\lvert U_{\mu 4}\rvert^2$	0.014	0.012	0.013	0.011
	$\sin^2 2\vartheta_{e\mu}$	0.0018	0.0018	0.0017	0.0017
	$\sin^2 2\vartheta_{ee}$	0.12	0.14	0.13	0.14
	$\sin^2 2\vartheta_{\mu\mu}$	0.054	0.049	0.05	0.045
Parameter goodness of fit	$\Delta\chi^2_{\rm min}$	15.8	15.8	9.3	9.2
	NDF	2	2	2	2
	GOF	4×10^{-4}	4×10^{-4}	0.01	0.01

or $|U_{\mu 4}|^2 \simeq 1$ and $\sin^2 2\vartheta_{e\mu} \simeq 4|U_{e4}|^2$, small values of $\sin^2 2\vartheta_{ee}$ and $\sin^2 2\vartheta_{\mu\mu}$ are allowed. On the other hand, in the global analysis values of $|U_{e4}|^2$ and $|U_{\mu 4}|^2$ close to unity are forbidden, respectively, by the observation of solar and atmospheric neutrino oscillations. In our analysis, we use the data of the very-long-baseline KamLAND reactor antineutrino experiment [56], which measured a disappearance of $\bar{\nu}_e$ due to Δm^2_{21}, which is compatible with solar neutrino oscillations. The KamLAND measurements require a relatively large value of $|U_{e1}|^2 + |U_{e2}|^2$, which by unitarity constrain $|U_{e4}|^2$ to be much smaller than unity (see Ref. [28]). In a similar way, the observation of atmospheric $\overset{(-)}{\nu}_\mu$ oscillations due to Δm^2_{31} requires relatively large values of $|U_{\mu 1}|^2 + |U_{\mu 2}|^2 + |U_{\mu 3}|^2$, which by unitarity constrain $|U_{\mu 4}|^2$ to be much smaller than unity. In our analysis, we use the bound on $|U_{\mu 4}|^2$ obtained in the analysis of atmospheric neutrino data presented in Ref. [37].

In Fig. 7, one can see that for $\Delta m^2_{41} \gtrsim 1$ eV^2 large values of $\sin^2 2\vartheta_{\mu\mu}$ are not allowed by the analysis of appearance data. The reason is that, as explained in Sec. II, we fit the MiniBooNE $\overset{(-)}{\nu}_\mu \to \overset{(-)}{\nu}_e$ data together with the MiniBooNE $\overset{(-)}{\nu}_\mu \to \overset{(-)}{\nu}_\mu$ data which have correlated uncertainties. The MiniBooNE $\overset{(-)}{\nu}_\mu \to \overset{(-)}{\nu}_\mu$ data constrain the disappearance of $\overset{(-)}{\nu}_\mu$'s for $\Delta m^2_{41} \gtrsim 1$ eV^2 [75], limiting the allowed value of $\sin^2 2\vartheta_{\mu\mu}$.

The last line of Table I gives the parameter goodness of fit [74] in the four analyses, which has been obtained by comparing the global best fit with the sum of the best fits of the appearance and disappearance data. We think that this parameter goodness of fit is more reliable than the parameter goodness of fit obtained by comparing data in favor and against short-baseline neutrino oscillations, which has been considered in several previous analyses, including ours [30]. The reason is that the distinction between appearance and disappearance data is made *a priori*, without considering the data. In this case, $\Delta\chi^2_{\rm min} = (\chi^2_{\rm min})_{\rm app+dis} - (\chi^2_{\rm min})_{\rm app} - (\chi^2_{\rm min})_{\rm dis}$ is a random variable with a χ^2 distribution with 2 degrees of freedom, as shown in Ref. [74]. On the other hand, comparing data in favor and against short-baseline neutrino oscillations one chooses the two sets of data in order to obtain always the worse $\Delta\chi^2_{\rm min}$ allowed by the data. In this case, $\Delta\chi^2_{\rm min}$ does not have a χ^2 distribution and the parameter goodness of fit is underestimated by assuming a χ^2 distribution with 2 degrees of freedom. Moreover, after the discovery of the reactor antineutrino anomaly [55] it is not clear if the reactor antineutrino data should be put in the group of experiments in which there is no evidence of short-baseline neutrino oscillations, as traditionally done, or in the group of experiments in favor of short-baseline neutrino oscillations. Therefore, we advocate the robust parameter goodness of fit [74] obtained from appearance and disappearance data.

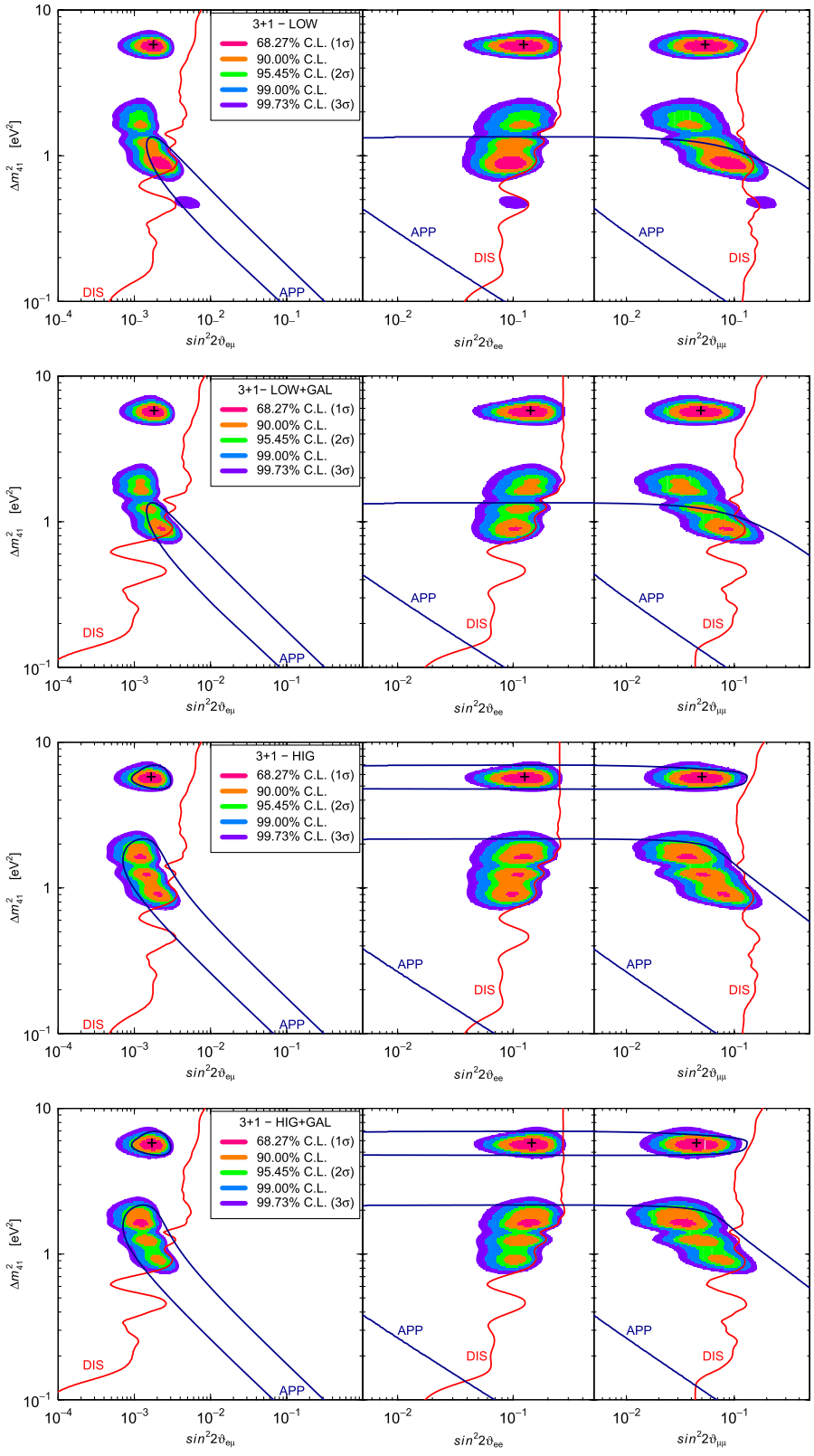

FIG. 7 (color online). Allowed regions in the $\sin^2 2\vartheta_{e\mu} - \Delta m^2_{41}$, $\sin^2 2\vartheta_{ee} - \Delta m^2_{41}$, and $\sin^2 2\vartheta_{\mu\mu} - \Delta m^2_{41}$ planes in the four cases listed in Table I. The best-fit points are indicated by crosses. The thick solid blue lines with the label APP show the 3σ allowed regions obtained from the analysis of $\overset{(-)}{\nu}_\mu \to \overset{(-)}{\nu}_e$ appearance data. The thick solid red lines with the label DIS show the 3σ allowed regions obtained from the analysis of disappearance data.

The values of such parameter goodness of fit listed in the last line of Table I show that there is a tension between appearance and disappearance data. This tension is severe in the two LOW fits. The reason can be understood by looking at the two corresponding panels in Fig. 7. One can see that for appearance data there is no 3σ allowed region around the best-fit point because the low-energy MiniBooNE data are not fitted well by such high values of Δm^2_{41} and small mixing. Hence, the best-fit point lies out of the region of overlap of the 3σ allowed regions of appearance and disappearance data. This is a symptom of a severe tension.

The tension between appearance and disappearance data is reduced in the HIG fits, for which there is a 3σ allowed region around the best-fit point, as one can see from the corresponding panels in Fig. 7. The resulting parameter goodness of fit, about 1%, is not large, but also not small enough to reject the fit with reasonable confidence.

Table I and Fig. 7 show that the Gallium data do not have a large impact on the results of the fit. The reason is that the data points are only four, much less than the reactor data points which give information on the same probability of ν_e and $\bar{\nu}_e$ disappearance. The main effect of Gallium data is to favor values of Δm^2_{41} larger than about 1eV^2. Indeed, in the HIG + GAL panel in Fig. 7 there are no regions allowed at 1σ below about $1.3\ \text{eV}^2$.

In comparison with the allowed regions of the 3 + 1 oscillation parameters obtained in Ref. [30], the inclusion in the analysis of the MINOS data discussed in Sec. III has the effect of disfavoring the regions with $\Delta m^2_{41} \lesssim 1\ \text{eV}^2$ and moving the best-fit value of Δm^2_{41} from the value of 0.9eV^2 obtained in Ref. [30] to $\Delta m^2_{41} \approx 5.6\ \text{eV}^2$.

V. CONCLUSIONS

The results of our analysis of short-baseline neutrino oscillation data show that the data can be fitted in the framework of 3 + 1 neutrino mixing, which requires the existence of a sterile neutrino with mass at the eV scale.

The fit has a tension due to the lack of observation of enough short-baseline disappearance of $\bar{\nu}_e$ and ν_μ to fully explain the $\bar{\nu}_\mu \to \bar{\nu}_e$ signal observed in the LSND and MiniBooNE experiments. However, we found that the appearance and disappearance data are marginally compatible if we neglect the data on the MiniBooNE low-energy anomaly, which may have an explanation different from $\overset{(-)}{\nu}_\mu \to \overset{(-)}{\nu}_e$ oscillations. In any case, we think that the neutrino oscillation explanation of the data cannot be dismissed with a light heart because besides the LSND and MiniBooNE indications in favor of a short-baseline $\bar{\nu}_\mu \to \bar{\nu}_e$ signal we have the reactor antineutrino anomaly [55] and the Gallium neutrino anomaly [65] in favor, respectively, of short-baseline $\bar{\nu}_e$ and ν_e disappearance, which could be due to the same squared-mass difference.

Since the recent MiniBooNE antineutrino data [31,32] do not show a large difference from the neutrino data [25], there is no serious motivation to consider the more complicated 3 + 2 neutrino mixing, which would allow for a possible *CP*-violating difference between neutrino and antineutrino transitions [27,29,30,34–37]. Moreover, as we have shown in Ref. [30], 3 + 2 mixing cannot resolve the tension between appearance and disappearance data. Finally, the hierarchical 3 + 1 scheme [see Eq. (1)] is favored over a hierarchical 3 + 2 scheme by standard ΛCDM analyses of cosmological data [14–19], which disfavor sums of neutrino masses much larger than 1 eV, and by big-bang nucleosynthesis data, which allow the existence of one sterile neutrino [20,21], but not more [19,22] (keeping however in mind the caveat that these bounds refer to the number of sterile neutrinos which have been fully thermalized in the early Universe).

Hence, in this paper we considered only 3 + 1 neutrino mixing, which is attractive for the natural correspondence of the existence of one new entity (a sterile neutrino) with the observation of a new effect (short-baseline oscillations).

The results of our fit excluding the MiniBooNE low-energy anomaly lead to a best fit at $\Delta m^2_{41} \approx 5.6\ \text{eV}^2$, which is larger than that obtained in Ref. [30] (about $0.9\ \text{eV}^2$) because of the new MINOS constraints discussed in Sec. III. The new best-fit value of Δm^2_{41} is rather large in comparison with the standard cosmological bounds [14–19] and may indicate the existence of nonstandard effects in the evolution of the Universe [19]. However, there are three regions within 1σ at $\Delta m^2_{41} \approx 1.6$, 1.2, $0.91\ \text{eV}^2$ which may be compatible with the standard cosmological bounds.

We have also shown that the data on the Gallium neutrino anomaly favor values of Δm^2_{41} larger than about $1\ \text{eV}^2$, but their impact is small because the results of the analysis are dominated by the more abundant reactor antineutrino data, which give information on the same probability of ν_e and $\bar{\nu}_e$ disappearance.

ACKNOWLEDGMENTS

We would like to thank Z. Djurcic, W. Louis, G. Mention, T. Schwetz, A. Smirnov, A. Sousa, and O. Yasuda for useful discussions.

[1] A. Aguilar *et al.* (LSND), Phys. Rev. D **64**, 112007 (2001).
[2] K. Abe *et al.* (Super-Kamiokande), Phys. Rev. D **83**, 052010 (2011).
[3] P. Adamson *et al.* (MINOS), Phys. Rev. Lett. **106**, 181801 (2011).
[4] S. Schael *et al.* (ALEPH, DELPHI, L3, OPAL, SLD, LEP Electroweak Working Group, SLD Electroweak Group, SLD Heavy Flavour Group), Phys. Rep. **427**, 257 (2006).
[5] S. M. Bilenky, C. Giunti, and W. Grimus, Prog. Part. Nucl. Phys. **43**, 1 (1999).
[6] M. Maltoni, T. Schwetz, M. Tortola, and J. Valle, New J. Phys. **6**, 122 (2004).
[7] A. Strumia and F. Vissani, arXiv:hep-ph/0606054.
[8] M. C. Gonzalez-Garcia and M. Maltoni, Phys. Rep. **460**, 1 (2008).
[9] G. L. Fogli *et al.*, Phys. Rev. D **78**, 033010 (2008).
[10] B. A. Reid, L. Verde, R. Jimenez, and O. Mena, J. Cosmol. Astropart. Phys. 01 (2010) 003.
[11] S. A. Thomas, F. B. Abdalla, and O. Lahav, Phys. Rev. Lett. **105**, 031301 (2010).
[12] M. C. Gonzalez-Garcia, M. Maltoni, and J. Salvado, J. High Energy Phys. 08 (2010) 117.
[13] M. Archidiacono, E. Calabrese, and A. Melchiorri, arXiv:1109.2767.
[14] J. Hamann, S. Hannestad, G. G. Raffelt, I. Tamborra, and Y. Y. Wong, Phys. Rev. Lett. **105**, 181301 (2010).
[15] E. Giusarma *et al.*, Phys. Rev. D **83**, 115023 (2011).
[16] J. R. Kristiansen and O. Elgaroy, arXiv:1104.0704 [Astron. Astrophys. (to be published)].
[17] Z. Hou, R. Keisler, L. Knox, M. Millea, and C. Reichardt, arXiv:1104.2333.
[18] A. X. Gonzalez-Morales, R. Poltis, B. D. Sherwin, and L. Verde, arXiv:1106.5052.
[19] J. Hamann, S. Hannestad, G. G. Raffelt, and Y. Y. Wong, J. Cosmol. Astropart. Phys. 09 (2011) 034.
[20] R. H. Cyburt, B. D. Fields, K. A. Olive, and E. Skillman, Astropart. Phys. **23**, 313 (2005).
[21] Y. I. Izotov and T. X. Thuan, Astrophys. J. **710**, L67 (2010).
[22] G. Mangano and P. D. Serpico, Phys. Lett. B **701**, 296 (2011).
[23] B. Armbruster *et al.* (KARMEN), Phys. Rev. D **65**, 112001 (2002).
[24] P. Astier *et al.* (NOMAD), Phys. Lett. B **570**, 19 (2003).
[25] A. A. Aguilar-Arevalo (MiniBooNE), Phys. Rev. Lett. **102**, 101802 (2009).
[26] A. A. Aguilar-Arevalo *et al.* (MiniBooNE), Phys. Rev. Lett. **105**, 181801 (2010).
[27] E. Akhmedov and T. Schwetz, J. High Energy Phys. 10 (2010) 115.
[28] C. Giunti and M. Laveder, Phys. Rev. D **83**, 053006 (2011).
[29] J. Kopp, M. Maltoni, and T. Schwetz, Phys. Rev. Lett. **107**, 091801 (2011).
[30] C. Giunti and M. Laveder, Phys. Rev. D **84**, 073008 (2011).
[31] E. Zimmerman (MiniBooNE), in Proceedings of PANIC, 2011 (unpublished).
[32] Z. Djurcic (MiniBooNE), in Proceedings of NUFACT, 2011 (unpublished).
[33] P. Adamson *et al.* (MINOS), Phys. Rev. Lett. **107**, 011802 (2011).
[34] M. Sorel, J. Conrad, and M. Shaevitz, Phys. Rev. D **70**, 073004 (2004).
[35] G. Karagiorgi *et al.*, Phys. Rev. D **75**, 013011 (2007).
[36] G. Karagiorgi, Z. Djurcic, J. Conrad, M. H. Shaevitz, and M. Sorel, Phys. Rev. D **80**, 073001 (2009).
[37] M. Maltoni and T. Schwetz, Phys. Rev. D **76**, 093005 (2007).
[38] P. Adamson *et al.* (MINOS) Phys. Rev. D **82**, 051102 (2010).
[39] K. Abe *et al.* (T2K), Phys. Rev. Lett. **107**, 041801 (2011).
[40] P. Adamson *et al.* (MINOS), Phys. Rev. Lett. **107**, 181802 (2011).
[41] G. L. Fogli, E. Lisi, A. Marrone, A. Palazzo, and A. M. Rotunno, Phys. Rev. D **84**, 053007 (2011).
[42] T. Schwetz, M. Tortola, and J. W. F. Valle, New J. Phys. **13**, 109401 (2011).
[43] D. Hernandez and A. Y. Smirnov, arXiv:1105.5946.
[44] P. Adamson *et al.* (The MINOS) Phys. Rev. D **81**, 052004 (2010).
[45] L. Loiacono, Ph.D. thesis, The University of Texas at Austin, 2010.
[46] A. Martin, W. Stirling, R. Thorne, and G. Watt, Eur. Phys. J. C **63**, 189 (2009).
[47] B. Achkar *et al.* (Bugey), Nucl. Phys. **B434**, 503 (1995).
[48] Y. Declais *et al.* (Bugey), Phys. Lett. B **338**, 383 (1994).
[49] A. Kuvshinnikov, L. Mikaelyan, S. Nikolaev, M. Skorokhvatov, and A. Etenko, JETP Lett. **54**, 253 (1991).
[50] G. Zacek *et al.* (CalTech-SIN-TUM) Phys. Rev. D **34**, 2621 (1986).
[51] A. Hoummada, S. Lazrak Mikou, G. Bagieu, J. Cavaignac, and D. Holm Koang, Appl. Radiat. Isot. **46**, 449 (1995).
[52] G. S. Vidyakin *et al.*, Sov. Phys. JETP **71**, 424 (1990).
[53] T. A. Mueller *et al.*, Phys. Rev. C **83**, 054615 (2011).
[54] P. Huber, Phys. Rev. C **84**, 024617 (2011).
[55] G. Mention *et al.*, Phys. Rev. D **83**, 073006 (2011).
[56] S. Abe *et al.* (KamLAND), Phys. Rev. Lett. **100**, 221803 (2008).
[57] F. Dydak *et al.* (CDHSW), Phys. Lett. **134B**, 281 (1984).
[58] P. Anselmann *et al.* (GALLEX), Phys. Lett. B **342**, 440 (1995).
[59] W. Hampel *et al.* (GALLEX), Phys. Lett. B **420**, 114 (1998).
[60] F. Kaether, W. Hampel, G. Heusser, J. Kiko, and T. Kirsten, Phys. Lett. B **685**, 47 (2010).
[61] J. N. Abdurashitov *et al.* (SAGE), Phys. Rev. Lett. **77**, 4708 (1996).
[62] J. N. Abdurashitov *et al.* (SAGE), Phys. Rev. C **59**, 2246 (1999).
[63] J. N. Abdurashitov *et al.* (SAGE), Phys. Rev. C **73**, 045805 (2006).
[64] J. N. Abdurashitov *et al.* (SAGE), Phys. Rev. C **80**, 015807 (2009).
[65] C. Giunti and M. Laveder, Phys. Rev. C **83**, 065504 (2011).
[66] J. N. Bahcall, P. I. Krastev, and E. Lisi, Phys. Lett. B **348**, 121 (1995).
[67] M. Laveder, Nucl. Phys. B, Proc. Suppl. **168**, 344 (2007).

[68] C. Giunti and M. Laveder, Mod. Phys. Lett. A **22**, 2499 (2007).
[69] C. Giunti and M. Laveder, Phys. Rev. D **77**, 093002 (2008).
[70] M. A. Acero, C. Giunti, and M. Laveder, Phys. Rev. D **78**, 073009 (2008).
[71] C. Giunti and M. Laveder, Phys. Rev. D **80**, 013005 (2009).
[72] C. Giunti and M. Laveder, Phys. Rev. D **82**, 053005 (2010).
[73] V. N. Gavrin, V. V. Gorbachev, E. P. Veretenkin, and B. T. Cleveland, arXiv:1006.210.
[74] M. Maltoni and T. Schwetz, Phys. Rev. D **68**, 033020 (2003).
[75] A. A. Aguilar-Arevalo *et al.* (MiniBooNE), Phys. Rev. Lett. **103**, 061802 (2009).